Eur. Phys. J. C (2025) 85:1025
https://doi.org/10.1140/epjc/s10052-025-14778-7

THE EUROPEAN PHYSICAL JOURNAL C

Regular Article - Theoretical Physics

Can decaying vacuum solve the H_0 tension?

L. S. Brito[1,a], **J. F. Jesus**[1,2,b], **A. A. Escobal**[1,3,4,c], **S. H. Pereira**[1,d]

[1] Universidade Estadual Paulista (UNESP), Faculdade de Engenharia e Ciências, Departamento de Física, Av. Dr. Ariberto Pereira da Cunha 333, Guaratinguetá, SP 12516-410, Brazil
[2] Universidade Estadual Paulista (UNESP), Instituto de Ciências e Engenharia, Departamento de Ciências e Tecnologia, R. Geraldo Alckmin, 519, Itapeva, SP 18409-010, Brazil
[3] Department of Astronomy, University of Science and Technology of China, Hefei 230026, Anhui, China
[4] Instituto de Astronomia, Geofísica e Ciências Atmosféricas, Universidade de São Paulo, São Paulo, SP 05508-900, Brazil

Received: 28 January 2025 / Accepted: 8 September 2025
© The Author(s) 2025

Abstract In the present work we analyze two different models of interaction between dark energy and dark matter, also known as vacuum decay models or $\Lambda(t)$CDM models. In both models, when the H_0 parameter is constrained by high-redshift data as the Planck distance priors (CMB) and transversal BAO, its value is compatible with a higher value of H_0, in agreement with low-redshift data, as Pantheon+&SH0ES (PS) and Cosmic Chronometers (CC). For one of the models, only a mild $\sim 2.1\sigma$ tension is found for Ω_m, which at least is an alleviation to the $\gtrsim 5\sigma$ H_0 tension in the context of standard ΛCDM model. We find $H_0 = 71.63 \pm 0.60$ km/s/Mpc for one model and $H_0 = 71.67 \pm 0.60$ km/s/Mpc for the other one, by combining CC+PS+BAO+CMB. We also find the decay parameter to be $\epsilon = 0.0162^{+0.0029}_{-0.0026}$ for one model and $\epsilon = 0.0209 \pm 0.0036$ for the other one. All constraints are at 68% c.l. From these analyses, a noninteracting model is excluded at least at 5.8σ c.l. We shall emphasize, however, that this result comes from an analysis that involves an approximated treatment to CMB, the Planck distance priors, as mentioned above. We have also verified that if the SH0ES prior is not included, the evidence for an interacting model decreases from 5.8σ to 4σ, a result closer to other recent works in the literature. This shows that these types of models are promising in solving or at least alleviating the H_0 tension problem.

1 Introduction

The ΛCDM model (formed by a Cold Dark Matter component plus a cosmological constant Λ) is currently the most widely accepted cosmological model to describe the evolution of the Universe, due to its ability to accurately describe key observational data, such as the cosmic microwave background (CMB) power spectrum and the accelerated expansion of the Universe. However, despite its success, the ΛCDM model faces several challenges, both theoretical and observational. Among these are the cosmological constant problem or Dark Energy (DE) problem, the nature of Dark Matter (DM), the coincidence problem and more recently the Hubble tension.

The cosmological constant problem arises from the discrepancy between theoretical predictions of vacuum energy from quantum field theory and the observed value of the vacuum energy density. Quantum Field Theory in curved spacetime predicts a vacuum energy density that is approximately 120 orders of magnitude larger than what is inferred from astronomical observations. This vast difference between the theoretical prediction and the observationally inferred value remains one of the greatest unsolved problems in modern Cosmology [1,2]. Another profound mystery in modern Cosmology is the nature of DM. Although it constitutes approximately 27% of the total mass-energy content of the Universe, dark matter does not interact with electromagnetic radiation, making it invisible to current detection methods. Its presence is inferred primarily through its gravitational effects, such as the rotation curves of galaxies and gravitational lensing. Despite extensive efforts to directly detect dark matter particles, their exact nature remains elusive. The coincidence problem, on the other hand, refers to the seemingly peculiar fact that the current densities associated with the DE or vac-

[a] e-mail: lucas.s.brito@unesp.br (corresponding author)
[b] e-mail: jf.jesus@unesp.br
[c] e-mail: anderson.aescobal@gmail.com
[d] e-mail: s.pereira@unesp.br

Published online: 19 September 2025

uum energy and DM are of the same order of magnitude, despite having evolved very differently throughout the history of the Universe. In the early Universe, the density of matter was vastly greater than that of dark energy. As the Universe expanded, dark matter density diluted, while dark energy remained constant. The challenge is to explain why, out of all possible epochs, we observe the Universe at a time when these densities appear so closely aligned [3].

In this work, however, we focus on another significant cosmological issue: the Hubble tension [4]. Early estimates of the Hubble constant (H_0), which describes the current expansion rate of the Universe, varied considerably. During the 1960s and 1970s, measurements ranged from 50 km/s/Mpc to 100 km/s/Mpc, mainly due to the limitations in observational techniques at that time. In the 1990s, the Hubble Space Telescope provided more precise estimates of H_0, leading to a period of significant improvement in measurements. The SH0ES (Supernovae, H_0 for the Dark Energy Equation of State) Program further refined the value of the H_0 through detailed analyses of parallax measurements, Cepheid variable stars, gravitational lensing, and Type Ia supernovae (SNe Ia). The SH0ES team determined H_0 to be 74.2 ± 3.6 km/s/Mpc [5], with subsequent studies improving the precision to 73.17 ± 0.86 km/s/Mpc [6]. This value will be referred to as the SH0ES H_0. In contrast, the Planck satellite mission, operated by the European Space Agency (ESA), used a different approach to measure the expansion rate of the Universe. By analyzing data from the CMB in combination with baryon acoustic oscillation (BAO) data, the Planck team derived a lower value of $H_0 = 67.4 \pm 0.5$ km/s/Mpc [7], which we refer to as the Planck H_0.

The discrepancy between the SH0ES and Planck measurements of H_0 has sparked a significant debate within the cosmology community, as both values are derived from highly robust and independent datasets. The SH0ES estimate is based on local or low-redshift observations, while the Planck value stems from early or high-redshift Universe data, under the assumption of the ΛCDM model. This discrepancy has now reached a 5.8σ significance level, posing a serious challenge to the ΛCDM framework. Since systematic errors have not been able to account for this tension, various theoretical models have been proposed to resolve the issue. These include modifications such as models with additional degrees of freedom in the dark energy sector, and other alternative cosmological proposals [4].

In the present paper we are interested to investigate the Hubble tension in a special class of DE models, namely models with a time-varying Λ [8–18]. In such models, some *ad hoc* time dependence for $\Lambda(t)$ is assumed or can also be derived from Quantum Mechanical arguments or by geometrical motivations. There is also a class of models which can be derived from fundamental quantum field theories calculations in curved spacetime, known as running vacuum models (RVM). The theoretical development of RVM within the framework of quantum field theory has been addressed in several works, including [19–21]. While the general form of RVM has been known for some time from semi-qualitative renormalization group analyses (see the early review [22] and references therein), only more recently have explicit quantum field theory computations provided rigorous derivations of these formulas, as discussed in the modern review [23]. Relatively recent phenomenological analyses of these models were carried out in the references [24–29].

In the context of running cosmological constant models, one of the first confrontations with observational data, specifically SNe Ia data, was presented in the works [30,31]. In these studies, semiclassical models were developed in which the running cosmological constant evolves smoothly, without fine-tuning, as a consequence of generic quantum effects near the Planck scale. It was demonstrated that, due to the decoupling phenomenon, low-energy effects are irrelevant for the running of the cosmological constant. Consequently, the approximate coincidence between the density parameters of dark matter and dark energy is not restricted to any specific epoch in the history of the Universe. Subsequently, similar models of interacting dark energy and dark matter were explored in detail in references [25] and [26]. These studies provided analytical solutions and extensive numerical analyses, incorporating a wide range of observational data, including SNe Ia, BAO, $H(z)$, LSS, and CMB measurements. In the first reference, the running vacuum model was identified as the most theoretically motivated and statistically favoured, with a confidence level of 3σ. These results were further supported by the computation of the Akaike and Bayesian information criteria. In the second reference, the Hubble tension was analyzed in the context of vacuum dynamics, showing that the values of H_0 inferred from CMB observations are more strongly favoured than those obtained from local measurements. In [28,29] it was shown a significantly better agreement of RVM as compared to the concordance model, including structure formation data.

Here we analyze two different models of interaction between dark energy and dark matter. The first model has been extensively studied in various contexts; however, in this work, we focus specifically on the H_0 tension. For the second proposed model, to the best of our knowledge, it is being investigated for the first time.

The paper is organized as follows. We describe the Friedmann equations with a time-dependent $\Lambda(t)$-term in Sect. 2, where we also obtain analytical solutions for $H(z)$ in different classes of models. In Sect. 3, we constrain the parameters of the models using CMB from Planck, Pantheon+&SH0ES SNe Ia, Cosmic Chronometers (CC) and BAO and also compare the decaying vacuum models with standard ΛCDM. In the analysis, we consider separately the constraints from low

redshift and high redshift data. Finally, we present our conclusions and final remarks in Sect. 4.

2 Cosmological equations for a varying Λ term

From the cosmological principle, which assures that the spatial distribution of matter in the Universe is uniformly homogeneous and isotropic when viewed on large scale, the Einstein field equations leads to the so-called Friedmann equations, given by:

$$H^2 = \frac{8\pi G\rho_T}{3} - \frac{k}{a^2}, \tag{1}$$

$$\frac{\ddot{a}}{a} = -\frac{4\pi G}{3}(\rho_T + 3p_T), \tag{2}$$

where ρ_T is the total energy density of the Universe, p_T is the total pressure and k is the spatial curvature, which we assume to be zero from now on. Taking into account different contributions to ρ_T and p_T, they are given by:

$$\rho_T = \rho_M + \rho_\Lambda + \rho_r, \tag{3}$$

$$p_T = p_\Lambda + p_r = -\rho_\Lambda + \frac{1}{3}\rho_r \tag{4}$$

where $\rho_M = \rho_d + \rho_b$ corresponds to the sum of dark matter energy density (ρ_d) plus baryons energy density (ρ_b), which are both pressureless ($p_M = 0$), ρ_Λ corresponds to the time-varying $\Lambda(t)$-term, (with $p_\Lambda = -\rho_\Lambda$) and ρ_r corresponds to radiation, (with $p_r = \frac{1}{3}\rho_r$). The continuity equations may be written as:

$$\dot{\rho}_b + 3H\rho_b = 0, \tag{5}$$

$$\dot{\rho}_r + 4H\rho_r = 0, \tag{6}$$

$$\dot{\rho}_d + 3H\rho_d = Q, \tag{7}$$

$$\dot{\rho}_\Lambda = -Q, \tag{8}$$

where Q is the interaction term between pressureless matter and vacuum. Equations (5) and (6) promptly yield the standard result $\rho_b = \rho_{b0}a^{-3}$ and $\rho_r = \rho_{r0}a^{-4}$. In order to solve for ρ_d and ρ_Λ, however, we need the explicity form of the interaction term Q. Since we knows that baryons and dark matter share the same equation of state (EOS), one might also write:

$$\dot{\rho}_M + 3H\rho_M = Q \tag{9}$$

for the total pressureless matter.

In the present work we will study two possible interaction terms, namely $Q = 3\epsilon H\rho_\Lambda$ (Model I) and $Q = 3\epsilon aH\rho_\Lambda$ (Model II). Thus, one could summarize both interaction terms in one equation:

$$Q = 3\epsilon a^n H\rho_\Lambda \tag{10}$$

where $n = 0$ or $n = 1$ for the Models I and II, respectively. Model I is interesting for dimensional reasons, as the interaction term has dimensions $\propto H\rho$. Model II is interesting because it corresponds to an exponential decay of Λ with respect to the scale factor, as we shall see below. In the following subsections, we study each of these cases separately.

2.1 Model I: $Q = 3\epsilon H\rho_\Lambda$ class of models

This model has already been studied by [25,32–34], in the context of a dark energy with a constant equation of state. In this case, by replacing $n = 0$ in Eq. (10), Eq. (8) can be written as:

$$\dot{\rho}_\Lambda = -3\epsilon H\rho_\Lambda \tag{11}$$

By changing to scale factor derivatives by using the relation $\frac{d}{dt} = \dot{a}\frac{d}{da} = aH\frac{d}{da}$, it can be written as:

$$\rho'_\Lambda(a) = -\frac{3\epsilon\rho_\Lambda(a)}{a} \tag{12}$$

where $'$ means $\frac{d}{da}$. This equation can easily be solved to:

$$\rho_\Lambda = \rho_{\Lambda 0}a^{-3\epsilon} \tag{13}$$

where $\rho_{\Lambda 0}$ is the current value of Λ density. This coincides with the so-called Generalized Chen-Wu model, where $\Lambda \propto a^{-n}$ [35,36]. By replacing Eq. (13) in Eq. (9), and changing to scale factor derivatives, we find:

$$\rho'_M(a) = -\frac{3\rho_M}{a} + 3\epsilon\rho_{\Lambda 0}a^{-1-3\epsilon}. \tag{14}$$

This equation can be solved to:

$$\rho_M(a) = \left(\rho_{M0} - \frac{\epsilon\rho_{\Lambda 0}}{1-\epsilon}\right)a^{-3} + \frac{\epsilon\rho_{\Lambda 0}}{1-\epsilon}a^{-3\epsilon}. \tag{15}$$

By replacing (13) and (15) in Friedmann equation (1) and changing to redshift z, we find

$$H^2 = H_0^2\left[\left(\Omega_M - \frac{\epsilon\Omega_\Lambda}{1-\epsilon}\right)(1+z)^3 + \frac{\Omega_\Lambda(1+z)^{3\epsilon}}{1-\epsilon} + \Omega_r(1+z)^4\right] \tag{16}$$

where $\Omega_i \equiv \frac{8\pi G\rho_{i0}}{3H_0^2}$ are the current density parameters and the normalization condition reads:

$$\Omega_M + \Omega_\Lambda + \Omega_r = 1. \tag{17}$$

2.2 Model II: $Q = 3\epsilon aH\rho_\Lambda$ class of models

In this case, $n = 1$ in Eq. (10) and Eq. (8) can be solved to:

$$\rho_\Lambda = \rho_{\Lambda *}e^{-3\epsilon a} \tag{18}$$

where

$$\rho_{\Lambda *} \equiv \rho_{\Lambda 0}e^{3\epsilon} \tag{19}$$

As one may see, Eq. (18) corresponds to an exponential decay of Λ with respect to the scale factor. This model has already been proposed by Rajeev [37]. Although being proposed decades ago, it has never been tested against observations, as we shall test below.

Replacing (18) and (19) into Eq. (9) and solving, we find:

$$\rho_M = \frac{\rho_{M0}}{a^3} + \frac{\rho_{\Lambda 0}}{9\epsilon^3 a^3}\left[P(\epsilon) - P(\epsilon a)e^{3\epsilon(1-a)}\right], \tag{20}$$

where the cubic polynomial $P(x)$ is defined as:

$$P(x) \equiv 9x^3 + 9x^2 + 6x + 2. \tag{21}$$

By replacing (18) and (20) together with radiation term into Friedmann equation (2) we find:

$$H^2 = \frac{8\pi G}{3}\left\{\frac{\rho_{M0}}{a^3} + \frac{\rho_{\Lambda 0}}{9\epsilon^3 a^3}\left[P(\epsilon) - P(\epsilon a)e^{3\epsilon(1-a)}\right] + \rho_{\Lambda 0}e^{3\epsilon(1-a)} + \rho_{r0}a^{-4}\right\} \tag{22}$$

or:

$$H^2 = \frac{8\pi G}{3}\left\{\frac{\rho_{M0}}{a^3} + \frac{\rho_{\Lambda 0}}{9\epsilon^3 a^3}\left[P(\epsilon) - Q(\epsilon a)e^{3\epsilon(1-a)}\right] + \rho_{r0}a^{-4}\right\}, \tag{23}$$

where $Q(x)$ is the quadratic polynomial:

$$Q(x) \equiv P(x) - 9x^3 = 9x^2 + 6x + 2. \tag{24}$$

Dividing (23) by H_0^2, we find:

$$E^2 \equiv \frac{H^2}{H_0^2} = \frac{\Omega_M}{a^3} + \frac{\Omega_\Lambda}{9\epsilon^3 a^3} \times \left[P(\epsilon) - Q(\epsilon a)e^{3\epsilon(1-a)}\right] + \Omega_r a^{-4}, \tag{25}$$

where $\Omega_i \equiv \frac{8\pi G\rho_{i0}}{3H_0^2}$ are the current density parameters and the normalization condition reads:

$$\Omega_M + \Omega_\Lambda + \Omega_r = 1. \tag{26}$$

In terms of z, we have:

$$E(z)^2 = \Omega_M(1+z)^3 + \frac{\Omega_\Lambda(1+z)^3}{9\epsilon^3}\left[P(\epsilon) - Q\left(\frac{\epsilon}{1+z}\right)e^{\frac{3\epsilon z}{1+z}}\right] + \Omega_r(1+z)^4. \tag{27}$$

3 Analysis and results

In Ref. [6], the SH0ES collaboration were able to improve the cosmic distance ladder by calibrating the period-luminosity relation with photometric measurements of 88 Cepheid variables in the core of the Small Magellanic Cloud. With this analysis, they were able to increase the foundation of the cosmic distance ladder from three to four calibrating galaxies, thereby obtaining a combined result of $H_0 = 73.17 \pm 0.86$ km/s/Mpc. With this result, as explained by [6], the local measurement of H_0 based on Cepheids and Type Ia Supernovae shows a 5.8σ tension with the value inferred from CMB in the context of a ΛCDM cosmology, $H_0 = 67.4 \pm 0.5$ km/s/Mpc [7]. As we intend to add the most recent SNe Ia compilation, Pantheon+, we have chosen to use the Pantheon+&SH0ES (PS) data as representing low reshift data, including constraints over H_0. In fact, [38] have found $H_0 = 73.6 \pm 1.1$ km/s/Mpc in the context of flat ΛCDM model, which already indicated a 5.1σ tension.

As another relevant low-redshift dataset, we chose to work with Cosmic Chronometers (CC) data, which is interesting because it is independent of cosmological models, relying only on Astrophysical assumptions. We have chosen as CC sample, the recent sample from Moresco et al., consisting of 32 $H(z)$ data with estimated statistical and systematic uncertainties [39].

Here, instead of working with the full CMB power spectrum, we work simply with the so-called distance priors from Planck [40], which consist on three cosmological quantities obtained from the Planck 2018 Monte Carlo chains and, as shown by [40], result in approximately the same constraints from the full spectrum, in the context of flat ΛCDM, OΛCDM and flat XCDM.

In order to complement the high-redshift data, we chose to work with Baryon Acoustic Oscillations (BAO) constraints, in the form of the transversal BAO data [41]. We chose this dataset because it is claimed to be less model-dependent, which is crucial for BAO analyses, since most of BAO constraints tend to be model-dependent, introducing biases towards standard models.

In all analyses we have assumed a flat prior over the free parameters: $\Omega_m \in [0, 1]$, $H_0 \in [10, 100]$ km/s/Mpc, $\Omega_b \in [0.02, 0.07]$ and $\epsilon \in [-0.5, 0.5]$. It is important to mention that we have also allowed for a negative range for ϵ. However, as we shall see below, this range will not be favoured when combining the the low-redshift data and high-redshift data. In order to sample the posteriors, we have used the software emcee[1] [42] and in order to plot the results, we have used the software getdist[2] [43].

3.1 Model I ($Q = 3\epsilon H\rho_\Lambda$) results

In Fig. 1 it is shown the results for Model I ($Q = 3\epsilon H\rho_\Lambda$). We chose to work with the combinations CC+Pantheon+&SH0ES as low redshift constraints and CC+BAO+CMB as high-redshift constraint. Although CC can not be considered as high redshift constraint, it helps with the convergence of the MC chains, even if it provides weak constraints. As can

[1] https://emcee.readthedocs.io/.

[2] https://getdist.readthedocs.io/.

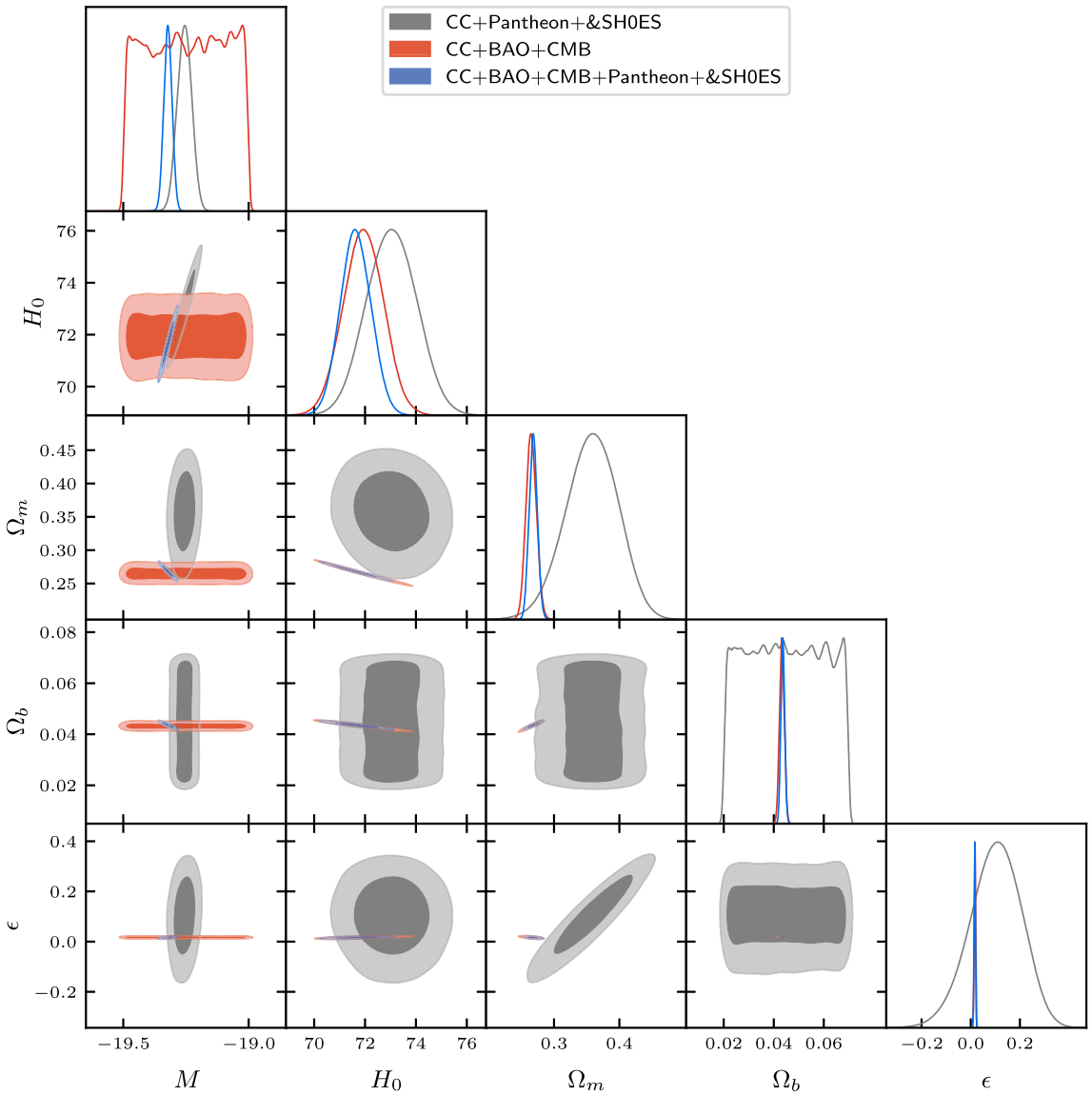


Fig. 1 Triangular plot of parameters, with data from Planck 2018 distance priors (CMB), Pantheon+&SH0ES, Cosmic Chronometers (CC) and transversal BAO for Model I (with $Q = 3\epsilon H\rho_\Lambda$). The contours correspond to 68% and 95% c.l

be seen from this Figure, the combination CC+BAO+CMB strongly constrain H_0, Ω_m, Ω_b and ϵ. It can be seen that $\epsilon > 0$ favours a higher value for H_0. Although most of the constraints are compatible for low and high redshift data, one may notice a slight tension for Ω_m: low-redhift data favour a higher value of Ω_m, while high-redshift data favour a lower value. In order to better quantify this tension, let us have a look at Table 1.

As can be seen from this Table, all parameters are compatible, except for Ω_m, where a small tension can be found of 2.2σ. Although being a significant tension, it is lower than the H_0 tension within ΛCDM of 5.1σ. We may say that the tension is alleviated within Model I. Figure 2 shows the combined constraints for Model I. A positive value for ϵ is favoured from this analysis.

3.2 Model II ($Q = 3\epsilon a H\rho_\Lambda$) results

In Fig. 3, we have the constraints for Model II ($Q = 3\epsilon a H\rho_\Lambda$). In general, the constraints are quite similar to Model I, but the high-redshift constraint over Ω_m seems to be slightly more consistent with the low-redshift constraint (Table 2).

As can be seen on this table, the values for all parameters are compatible between low-redshift and high-redshift data, except for Ω_m, where a 2.1σ tension was found. Again, we

Table 1 Numerical results for Model I. Mean values of the free parameters from the various combinations of datasets, together with the 1σ c.l. intervals

Dataset	H_0 (km/s/Mpc)	Ω_m	Ω_b	ϵ
CC+PP	67.5 ± 3.6	$0.344^{+0.047}_{-0.040}$	0.045 ± 0.014	$0.04^{+0.14}_{-0.11}$
CC+PS	73.05 ± 0.97	$0.358^{+0.042}_{-0.038}$	0.045 ± 0.014	$0.101^{+0.11}_{-0.097}$
CC+BAO+CMB	71.93 ± 0.79	$0.2650^{+0.0075}_{-0.0084}$	0.04322 ± 0.00094	$0.0170^{+0.0031}_{-0.0027}$
CC+PP+BAO+CMB	70.51 ± 0.70	0.2800 ± 0.0077	0.04493 ± 0.00090	0.0132 ± 0.0032
CC+PS+BAO+CMB	71.63 ± 0.60	0.2682 ± 0.0062	0.04361 ± 0.00075	$0.0162^{+0.0029}_{-0.0026}$

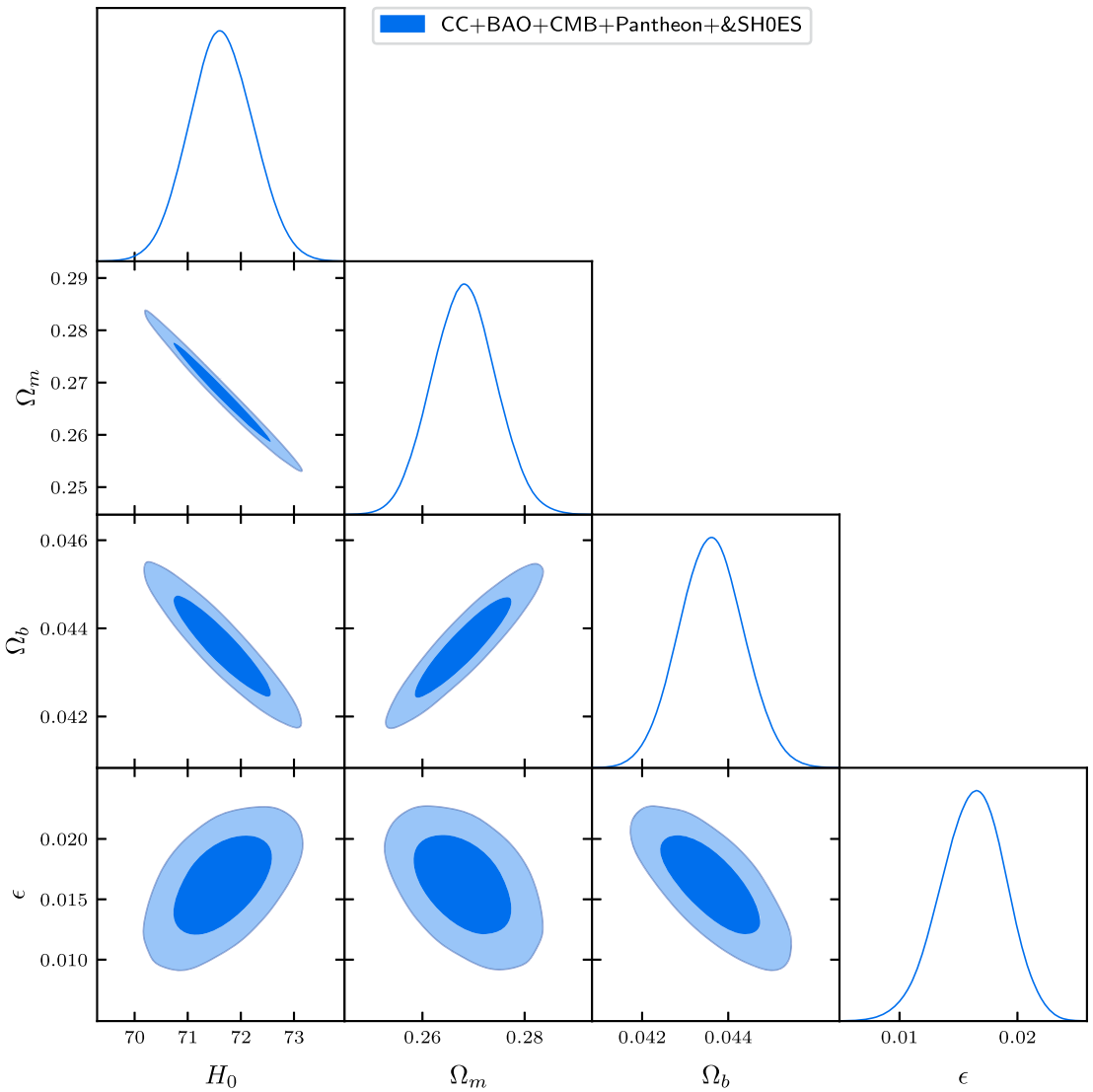


Fig. 2 Triangular plot of parameters for the joint analysis of CC+BAO+CMB+Pantheon+&SH0ES for Model I (with $Q = 3\epsilon H \rho_\Lambda$). The contours correspond to 68% and 95% c.l

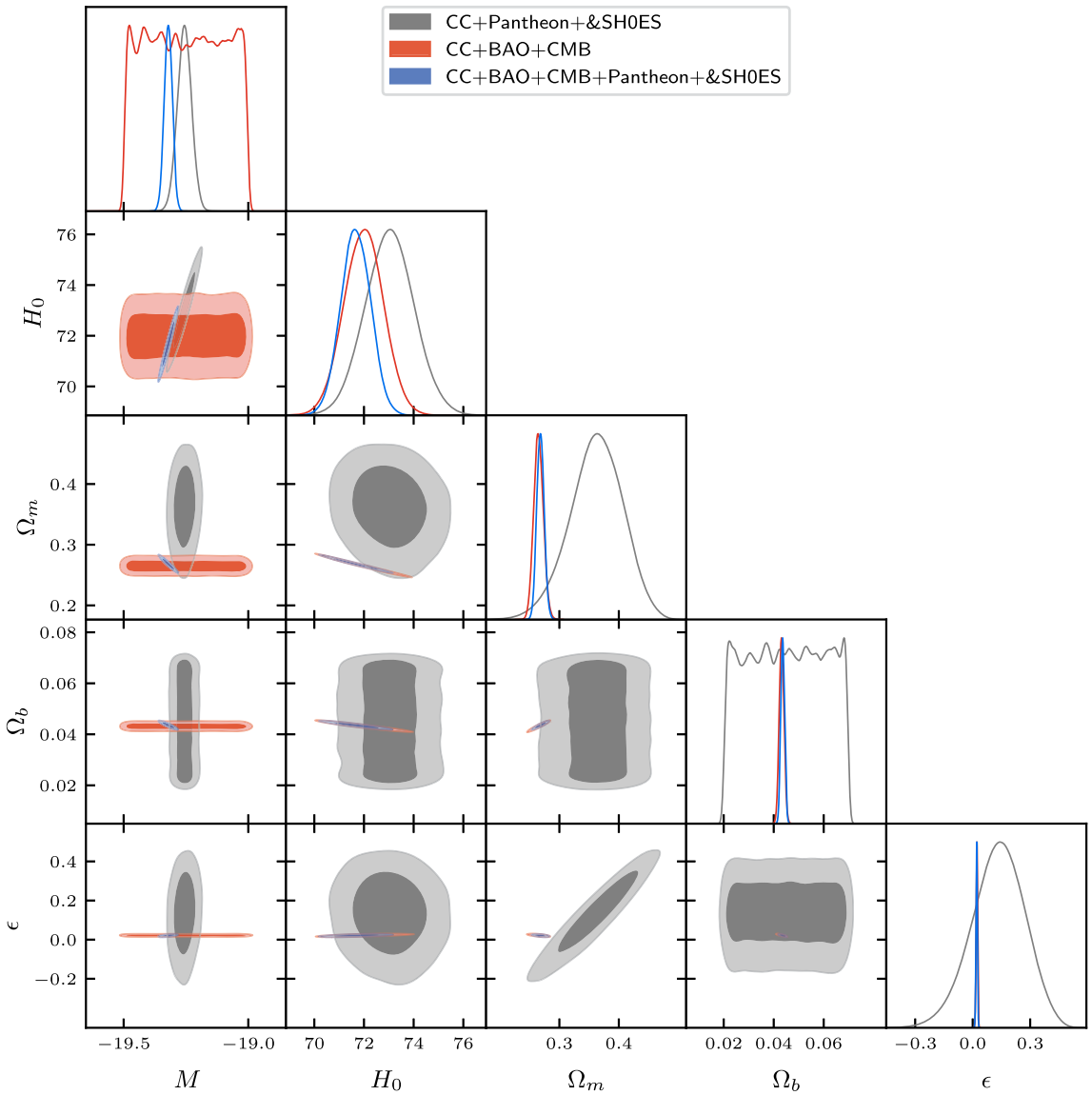


Fig. 3 Triangular plot of parameters, with data from Planck 2018 distance priors (CMB), Pantheon+&SH0ES, Cosmic Chronometers (CC) and transversal BAO for Model II (with $Q = 3\epsilon a H \rho_\Lambda$). The contours correspond to 68% and 95% c.l

Table 2 Numerical results for Model II. Mean values of the free parameters from the various combinations of datasets, together with the 1σ c.l. intervals

Dataset	H_0 (km/s/Mpc)	Ω_m	Ω_b	ϵ
CC+PP	67.5 ± 3.6	$0.347^{+0.052}_{-0.045}$	0.045 ± 0.014	$0.05^{+0.17}_{-0.15}$
CC+PS	73.04 ± 0.98	$0.362^{+0.048}_{-0.041}$	0.045 ± 0.015	$0.13^{+0.15}_{-0.13}$
CC+BAO+CMB	71.99 ± 0.79	0.2650 ± 0.0080	0.04316 ± 0.00095	$0.0221^{+0.0040}_{-0.0035}$
CC+PP+BAO+CMB	70.51 ± 0.72	0.2804 ± 0.0078	0.04494 ± 0.00092	0.0170 ± 0.0042
CC+PS+BAO+CMB	71.67 ± 0.60	0.2683 ± 0.0061	0.04357 ± 0.00075	0.0209 ± 0.0036

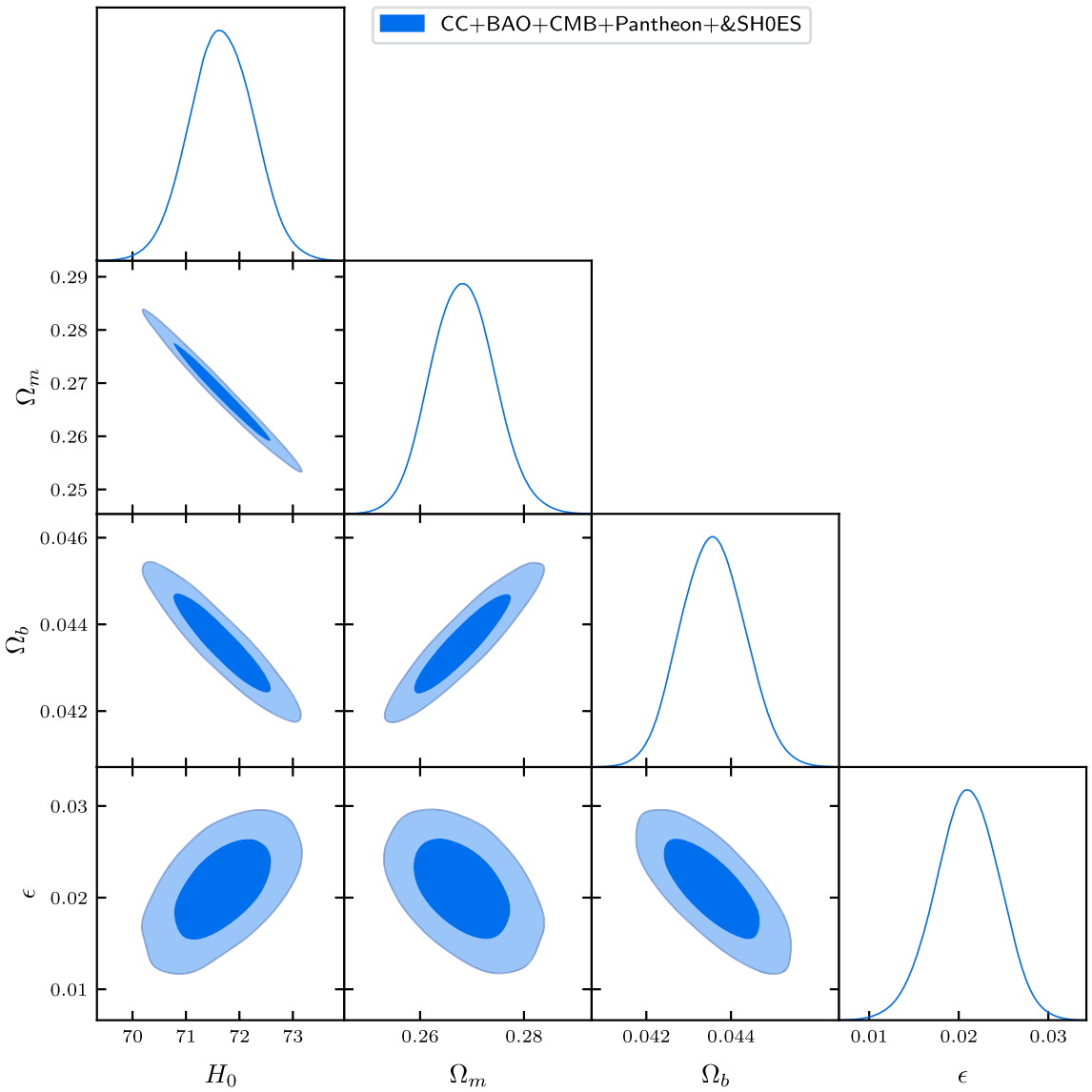


Fig. 4 Triangular plot of parameters for the joint analysis of CC+BAO+CMB+Pantheon+&SH0ES for Model II (with $Q = 3\epsilon a H \rho_\Lambda$). The contours correspond to 68% and 95% c.l

may say that the H_0 tension is transferred and alleviated to Ω_m (Fig. 4).

Note that the value for $\epsilon = 0.0162^{+0.0029}_{-0.0026}$ for Model I excludes a noninteracting model with $\sim 6.2\sigma$ c.l. The situation is quite similar for Model II, where $\epsilon = 0.0209 \pm 0.0036$ excludes a noninteracting model at $\sim 5.8\sigma$.

There are some analyses available in the literature concerning Model I. Bernui et al. [44] analyse a model similar to Model I, as they assume a dark energy with EOS $w = -0.9999$. By comparing the model with Planck data only, they find $\epsilon = -0.43^{+0.28}_{-0.21}$[3] and $H_0 = 71.7^{+2.3}_{-2.7}$ km/s/Mpc at 68% c.l. By comparing the model with Planck+transversal BAO+H_0, they find $\epsilon = -0.58 \pm 0.11$ and $H_0 = 73.99 \pm 0.88$ km/s/Mpc at 68% c.l. The H_0 values obtained from [44] are compatible with our analysis. The value they have obtained, however, for the ϵ parameter are incompatible with our analysis and also indicates a decay of DM into DE, differently of what we obtained here, that is, a decay of Λ into DM. The possible reasons for this difference is the fact that they have made an analysis with DE perturbation, which does not make sense for our model, as Λ is expected to be smooth. They also have used different data from the current analysis, that is, the full Planck CMB power spectrum and transversal BAO data.

[3] Their parameter ξ corresponds to ϵ from our analysis.

3.3 ΛCDM comparison

In order to compare the results we have obtained for these $\Lambda(t)$CDM model with the standard ΛCDM model, in this subsection we first perform the same analysis in the context of spatially flat ΛCDM model. The results of our analysis can be seen on Fig. 5.

As can be seen from Fig. 5, the constraints over H_0 from low redshift (mainly SH0ES) and high redshift (mainly CMB) are quite distant, with low redshift data favouring a high value for H_0, while high redshift data favours a low value for H_0, as well known in the context of H_0 tension. In this same figure, we also show the joint analysis, but in reality, it is meaningless, due to the high discrepancies obtained. The exact numerical results can be seen on Table 3.

As can be seen on Table 3, there was a high incompatibility between the H_0 constraints. In fact, the H_0 tension between CC+PS and CC+BAO+CMB was 3.7σ. This is lower than the usual tensions mentioned in the literature due to the fact that the transversal BAO alleviates the H_0 tension in the context of ΛCDM model, as already shown by [44].

In order to compare more directly the interacting models with ΛCDM, let us calculate two information criteria, namely, the AIC (Akaike Information Criterion) and BIC (Bayesian Information Criterion). As explained, for instance, in [45,46], the AIC can be written as

$$\mathrm{AIC} = -2\ln\mathcal{L}_{max} + 2p \tag{28}$$

where $\mathcal{L}_{max}$ is the maximum of the posterior distribution and p is the number of parameters. While AIC is an interesting tool for comparison between models, it is taken as not penalizing too much the excess of parameters. In order to further penalize the excess of parameters, it was defined the BIC, which is considered as an approximation of the Bayesian Evidence. The BIC can be written as [45,47]

$$\mathrm{BIC} = -2\ln\mathcal{L}_{max} + p\ln n \tag{29}$$

where n is number of data. The results for AIC and BIC as well for $\chi^2_\nu \equiv \frac{\chi^2_{min}}{n-p}$, can be seen on Table 4.

As can be seen on Table 4, although the χ^2_ν is similar for the three models analysed here, the χ^2_{min} for ΛCDM is too high when compared to Models I and II, in such a way that even if AIC and BIC penalize the excess of parameters of Models I and II, they still have advantage against ΛCDM. According to [45], a value of $\Delta\mathrm{AIC} > 10$ and $\Delta\mathrm{BIC} > 5$ is decisive against the model in question. So, we may conclude that both Model II and flat ΛCDM model can be discarded by the current analysis.

3.4 Comparison with other interacting models and analyses

The results obtained here departs markedly from earlier running–vacuum work. With a positive interaction strength $\epsilon \simeq 0.02$ from both models – meaning a small energy flow from vacuum to dark matter – the combined CC+Pantheon+&SH0ES+BAO+Planck data yield $H_0 = 71.6 \pm 0.6$ km/s/Mpc and rule out $\epsilon = 0$ at $\sim 6\sigma$. This lifts the CMB-based value of H_0 into full agreement with the local distance-ladder measurement while leaving only a mild ($\sim 2\sigma$) residual tension in Ω_m. By contrast, in the running-vacuum models of Solà and collaborators [25,26], a much smaller parameter $\nu \sim 10^{-3}$ is obtained; their global fits favour $H_0 \approx 67$–68 km s^{-1} Mpc^{-1} (close to Planck) and ease the σ_8 discrepancy. The early RG analyses of Shapiro et al. [31] and España-Bonet et al. [30] anticipated a natural percent-level running ($\nu \sim 0.02$) but lacked data to test it. More recent RVM analyses, however, already have favoured interacting models over the ΛCDM model. In Ref. [24], the so-called Type-I RRVM model with vacuum decay but no G variation, is analysed against SNe Ia+SH0ES+BAO+$H(z)$+LSS+Planck data. From this analysis, they have found $\nu_{eff} = -0.00005^{+0.00040}_{-0.00038}$ as interacting parameter. Therefore, in this scenario, a noninteracting model with $\nu_{eff} = 0$ can not be discarded. However, by adding a switch at $z_* \sim 1$ for the same type of interaction, defining what they call a threshold Type-I RRVM, they find $\nu_{eff} = 0.0209^{+0.0055}_{-0.0059}$, thereby discarding $\nu_{eff} = 0$ at 3.5σ. More recently [27], the same models were analysed against Pantheon+&SH0ES+BAO+$H(z)$+LSS+Planck data, and they have found $\nu_{eff} = -0.00037 \pm 0.00029$ for the Type-I RRVM and $\nu_{eff} = 0.0197 \pm 0.0055$ for the threshold Type-I RVM model. Again, ν_{eff} could not be discarded in the Type-I RRVM scenario, while in the Type-I RRVM scenario, the ΛCDM model could be discarded at 3.6σ c.l.

By comparing our analysis with these recent works, we may conclude that the models studied here are simpler and are better favoured against ΛCDM, concerning the H_0 tension. On the other hand, these recent RVM studies are more complete, in the sense that they use the full Planck likelihood and LSS data, and also in the sense that they attack both H_0 and σ_8 tensions.

More recently, while the present work was in the submission stage and we were improving and extending the analysis, a new paper has been published [48], based on our original proposal of studying these models. In [48], they have studied the Models I and II. However, their analysis is slightly different concerning the CC dataset, where we have used 32 $H(z)$ data from [39] and they have used just 31 $H(z)$ data from various references. Concerning the CMB distance prior, we are unable to compare their analysis with the present analysis, as they do not claim which distance prior they have chosen to use from Ref. [40]. In the present work, we have chosen to

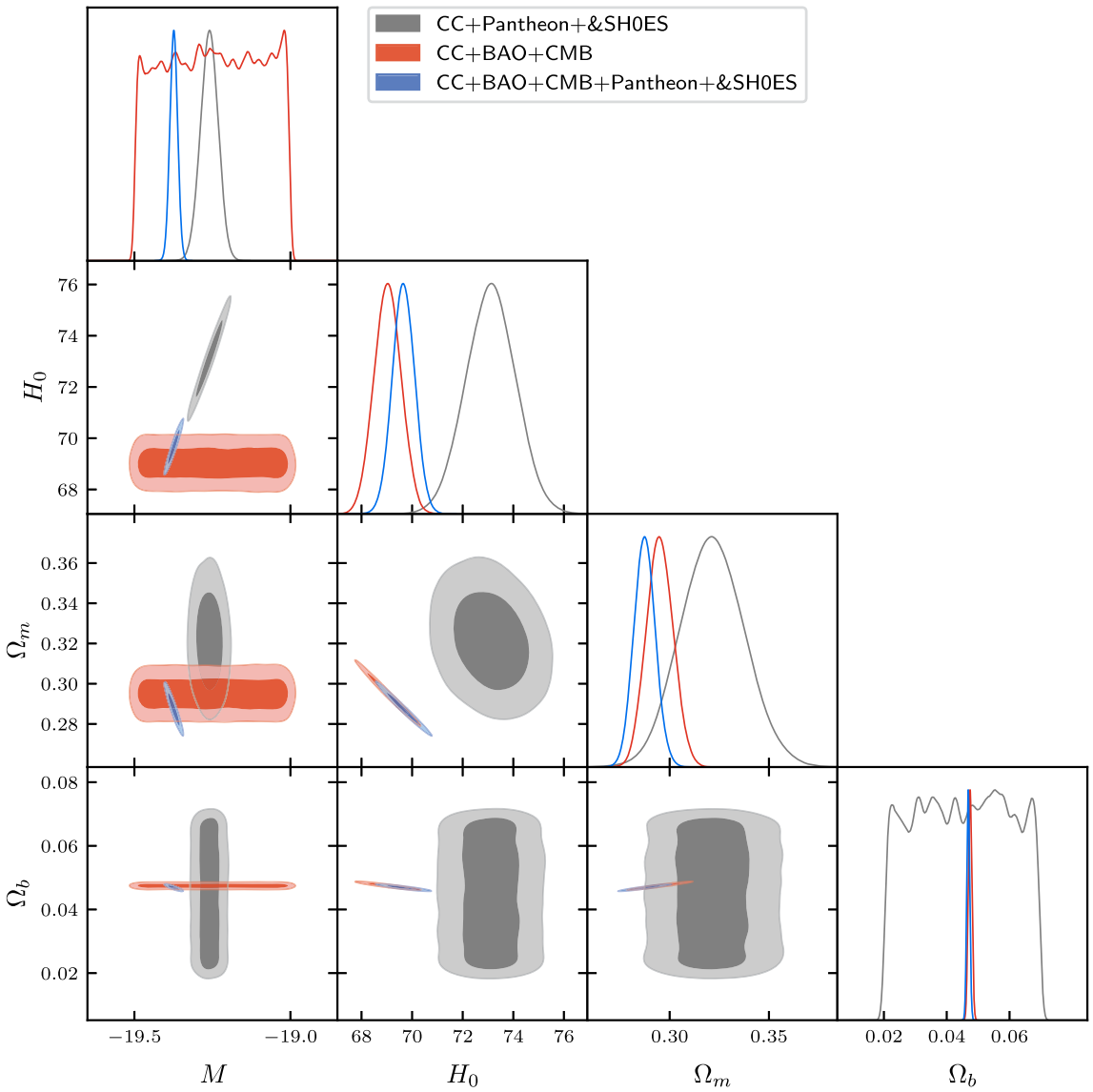


Fig. 5 Triangular plot of parameters, with data from Planck 2018 distance priors (CMB), Pantheon+&SH0ES, Cosmic Chronometers (CC) and transversal BAO for flat ΛCDM model. The contours correspond to 68% and 95% c.l

Table 3 Numerical results for flat ΛCDM model. Mean values of the free parameters from the various combinations of datasets, together with the 1σ c.l. intervals

Dataset	H_0 (km/s/Mpc)	Ω_m	Ω_b
CC+PP	67.0 ± 3.4	0.331 ± 0.018	0.045 ± 0.014
CC+PS	73.08 ± 0.98	0.322 ± 0.016	0.045 ± 0.015
CC+BAO+CMB	69.02 ± 0.52	0.2953 ± 0.0067	0.04747 ± 0.00056
CC+PP+BAO+CMB	68.66 ± 0.49	0.2999 ± 0.0064	0.04783 ± 0.00054
CC+PS+BAO+CMB	69.66 ± 0.44	0.2874 ± 0.0054	0.04686 ± 0.00047

Table 4 Comparison among the interacting models (I and II) and flat ΛCDM model

Model	χ^2_ν	AIC	ΔAIC	BIC	ΔBIC
I	0.8910	1514.1511	0	1541.3548	0
II	0.8853	1526.6273	12.4762	1553.8398	12.485
Flat ΛCDM	0.9012	1540.1878	26.0369	1561.9507	20.5959

work only with the flat ΛCDM distance prior. However, we do not expect to find an appreciable difference for changing the distance prior to wCDM for instance, as these priors are quite similar. Despite these slight differences, when we compare the SNe Ia data we have used in the present work with the one by [48], the difference is huge: They have used the Pantheon compilation [49], which contains only 1048 SNe Ia data and do not constrain H_0 alone, while we have used Pantheon+&SH0ES [38], which consists of 1701 light curves of 1550 distinct SNe Ia, and strongly constrains H_0. In [48], they have found a 2.8σ evidence for an interaction in the context of Model I and 2.6σ evidence for interaction in the context of Model II. Since we have found at least a $\sim 5.8\sigma$ evidence for interaction in the context of these models, we attribute this difference to the fact that we have used Pantheon+&SH0ES, which strongly constrains H_0, while [48] have chosen not to use H_0 constraints from SH0ES in their analysis. In order to better compare our current analysis with the one performed by [48], we have included an analysis without the SH0ES prior. That is, we performed an analysis replacing the Pantheon+&SH0ES compilation by the Pantheon+ compilation. The results can be seen on Tables 1, 2 and 3. In these tables, we have referred to the Pantheon+ sample as 'PP'. As can be seen from these tables, for Model I, the value obtained for the interaction parameter is $\epsilon = 0.0132 \pm 0.0032$, which shows a reduction from 5.9σ to 4.1σ when the Pantheon+&SH0ES is replaced by Pantheon+ compilation. In the case of Model II, we can see that the obtained result of $\epsilon = 0.0170 \pm 0.0042$ also shows an weaker evidence for interaction. That is, we have an evidence for interaction of 4σ, as compared to 5.8σ evidence when including the Pantheon+&SH0ES compilation. These results are closer to the results of 2.8σ for Model I and 2.6σ for Model II obtained by [48]. The remaining difference can be attributed to the fact that they have used an older sample of SNe Ia, Pantheon [49].

It is also important to note that [48] have used the DESI DR1 BAO data [50], while we have chosen to use the transversal BAO data [41]. It is important to mention that while DESI uses 3D BAO, the transversal BAO data consists of 2D BAO. In recent works [51,52], both analyses have been made in the context of dynamical dark energy models, and a higher evidence were found for dynamical dark energy in the case of 2D BAO. The fact that we have chosen to use 2D BAO in the present work may also contribute to a higher evidence of dark matter-quantum vacuum interaction. This has also appeared on Ref. [44], where they have shown that the H_0 tension disappears in the context of Model I by using 2D BAO data, while it is only alleviated when using 3D BAO. We have to remember, however, that the 2D BAO data is weakly dependent of cosmological models, as mentioned by [41], which makes it more suitable to analyse alternative models as Models I and II.

4 Conclusion

We have analysed the Hubble tension within the context of dark energy models with a time-varying cosmological constant, specifically vacuum decay models. The results obtained in this work show that vacuum decay models $\Lambda(t)$CDM, with interaction between dark matter and the cosmological parameter, are promising in addressing the Hubble H_0 tension. Our results show that vacuum decay models can reconcile the H_0 estimates, providing higher values in alignment with the low-redshift, Pantheon+&SH0ES data. It is clear from our analysis that the decay parameter ϵ allows H_0 to reach higher values for the high-redshift constraints, thereby reconciling high-redshift constraints with the local value for H_0. As a result of the interaction, however, for both models, a higher value for Ω_m is predicted from low-redshift data and a lower value for Ω_m is predicted from high-redshift data. This tension is around 2σ, representing a transfer and an alleviation of the H_0 tension. Due to the positive correlation between ϵ and H_0, a higher value for H_0 results in a positive value for ϵ, according to our analysis. From a thermodynamic point of view it is well known that this is the preferred direction of decay, as it does not require a non-vanishing chemical potential in the dark sector [32]. This suggests that the energy flow from vacuum to matter can be compatible with a higher H_0. We have to recall, however, that the present analysis was performed only with 2D BAO data, while it is known in the literature, as pointed by [51], that there is a conflict between 2D and 3D BAO data.

Our analysis have shown an evidence for an interaction between Λ and dark matter in the range of 5.8 to 5.9σ when we included all analysed datasets, that is, CC+PS+2D BAO+CMB priors. In order to test the impact of the SH0ES prior over our analysis, we have also performed an analysis excluding SH0ES data from the combination, that is, including only CC+PP+2D BAO+CMB priors. In this case, the range of evidence for an interacting model decreases to 4 to 4.1σ, a result closer to other recent works in the literature [48].

Although still showing some tension concerning the matter density parameter, our study shows that interacting models can be a promising direction to solve the H_0 tension. Therefore, it would be interesting, in the future, that a full CMB and LSS analyses (including 3D BAO data) would be performed in the context of these models, thereby providing a more definitive conclusion about the ability of $\Lambda(t)$CDM of solving or alleviating not only the H_0 tension, but also the σ_8 tension.

Acknowledgements This study was financed in part by the Coordenação de Aperfeiçoamento de Pessoal de Nível Superior - Brasil (CAPES) - Finance Code 001. JFJ acknowledges financial support from Conselho Nacional de Desenvolvimento Científico e Tecnológico (CNPq) (No. 314028/2023-4). SHP acknowledges financial support

from Conselho Nacional de Desenvolvimento Científico e Tecnológico (CNPq) (No. 308469/2021 and 301775/2025-7). We are also grateful to the referee for his/her valuable comments and suggestions that helped us to extend and improve the present work.

Data Availability Statement This manuscript has no associated data. [Authors' comment: The data used in this work are publicly avaliable.]

Code Availability Statement Code/software will be made available on reasonable request . [Authors' comment: The code/software generated during and/or analysed during the current study is available from the corresponding author on reasonable request.]

Open Access This article is licensed under a Creative Commons Attribution 4.0 International License, which permits use, sharing, adaptation, distribution and reproduction in any medium or format, as long as you give appropriate credit to the original author(s) and the source, provide a link to the Creative Commons licence, and indicate if changes were made. The images or other third party material in this article are included in the article's Creative Commons licence, unless indicated otherwise in a credit line to the material. If material is not included in the article's Creative Commons licence and your intended use is not permitted by statutory regulation or exceeds the permitted use, you will need to obtain permission directly from the copyright holder. To view a copy of this licence, visit http://creativecommons.org/licenses/by/4.0/.
Funded by SCOAP[3].

References

1. L. Perivolaropoulos, F. Skara, New Astron. Rev. **95**, 101659 (2022). arXiv:2105.05208 [astro-ph.CO]
2. S. Weinberg, Rev. Mod. Phys. **61**, 1–23 (1989)
3. H.E.S. Velten, R.F. Marttens, W. Zimdahl, Eur. Phys. J. C **74**(11), 3160 (2014). arXiv:1410.2509 [astro-ph.CO]
4. E. Valentino, O. Mena, S. Pan, L. Visinelli, W. Yang, A. Melchiorri, D.F. Mota, A.G. Riess, J. Silk, Class. Quantum Gravity **38**(15), 153001 (2021). arXiv:2103.01183 [astro-ph.CO]
5. A.G. Riess, L. Macri, S. Casertano, M. Sosey, H. Lampeitl, H.C. Ferguson, A.V. Filippenko, S.W. Jha, W. Li, R. Chornock et al., Astrophys. J. **699**, 539–563 (2009). arXiv:0905.0695 [astro-ph.CO]
6. L. Breuval, A.G. Riess, S. Casertano, W. Yuan, L.M. Macri, M. Romaniello, Y.S. Murakami, D. Scolnic, G.S. Anand, I. Soszyński, Astrophys. J. **973**(1), 30 (2024). arXiv:2404.08038 [astro-ph.CO]
7. N. Aghanim et al. [Planck], Astron. Astrophys. **641**, A6 (2020). arXiv:1807.06209 [astro-ph.CO]. [erratum: Astron. Astrophys. 652 (2021), C4]
8. A.M. Öztaş, Mon. Not. Roy. Astron. Soc. **481**(2), 2228–2234 (2018)
9. R.G. Vishwakarma, Class. Quantum Gravity **18**, 1159–1172 (2001). arXiv:astro-ph/0012492
10. J.M. Overduin, F.I. Cooperstock, Phys. Rev. D **58**, 043506 (1998). arXiv:astro-ph/9805260
11. H. Azri, A. Bounames, Int. J. Mod. Phys. D **26**(7), 1750060 (2017). arXiv:1412.7567 [gr-qc]
12. H. Azri, A. Bounames, Gen. Relativ. Gravit. **44**, 2547–2561 (2012). arXiv:1007.1948 [gr-qc]
13. M. Szydłowski, Phys. Rev. D **91**(12), 123538 (2015). arXiv:1502.04737 [astro-ph.CO]
14. M. Bruni, R. Maier, D. Wands, Phys. Rev. D **105**(6), 063532 (2022). arXiv:2111.01765 [gr-qc]
15. G. Papagiannopoulos, P. Tsiapi, S. Basilakos, A. Paliathanasis, Eur. Phys. J. C **80**(1), 55 (2020). arXiv:1911.12431 [gr-qc]
16. M. Benetti, W. Miranda, H.A. Borges, C. Pigozzo, S. Carneiro, J.S. Alcaniz, JCAP **12**, 023 (2019). arXiv:1908.07213 [astro-ph.CO]
17. M. Benetti, H. Borges, C. Pigozzo, S. Carneiro, J. Alcaniz, JCAP **08**, 014 (2021). arXiv:2102.10123 [astro-ph.CO]
18. H.A.P. Macedo, L.S. Brito, J.F. Jesus, M.E.S. Alves, Eur. Phys. J. C **83**(12), 1144 (2023). arXiv:2305.18591 [astro-ph.CO]
19. C. Moreno-Pulido, J. Sola, Eur. Phys. J. C **80**(8), 692 (2020). arXiv:2005.03164 [gr-qc]
20. C. Moreno-Pulido, J. Sola Peracaula, Eur. Phys. J. C **82**(6), 551 (2022). arXiv:2201.05827 [gr-qc]
21. C. Moreno-Pulido, J. Sola Peracaula, S. Cheraghchi, Eur. Phys. J. C **83**(7), 637 (2023). arXiv:2301.05205 [gr-qc]
22. J. Sola, J. Phys. Conf. Ser. **453**, 012015 (2013). arXiv:1306.1527 [gr-qc]
23. J. Sola Peracaula, Philos. Trans. Roy. Soc. Lond. A **380**, 20210182 (2022). arXiv:2203.13757 [gr-qc]
24. J. Solà Peracaula, A. Gómez-Valent, J. Cruz Perez, C. Moreno-Pulido, EPL **134**(1), 19001 (2021). arXiv:2102.12758 [astro-ph.CO]
25. J. Solà Peracaula, J. Cruz Pérez, A. Gomez-Valent, Mon. Not. Roy. Astron. Soc. **478**(4), 4357–4373 (2018). arXiv:1703.08218 [astro-ph.CO]
26. J. Solà, A. Gómez-Valent, J. Cruz Pérez, Phys. Lett. B **774**, 317–324 (2017). arXiv:1705.06723 [astro-ph.CO]
27. J. Sola Peracaula, A. Gomez-Valent, J. Cruz Perez, C. Moreno-Pulido, Universe **9**(6), 262 (2023). arXiv:2304.11157 [astro-ph.CO]
28. J. Solà, A. Gómez-Valent, J. Cruz Pérez, Astrophys. J. **836**(1), 43 (2017). arXiv:1602.02103 [astro-ph.CO]
29. J. Sola, A. Gomez-Valent, J. Cruz Pérez, Astrophys. J. Lett. **811**, L14 (2015). arXiv:1506.05793 [gr-qc]
30. C. Espana-Bonet, P. Ruiz-Lapuente, I.L. Shapiro, J. Sola, JCAP **02**, 006 (2004). arXiv:hep-ph/0311171
31. I.L. Shapiro, J. Sola, C. Espana-Bonet, P. Ruiz-Lapuente, Phys. Lett. B **574**, 149–155 (2003). arXiv:astro-ph/0303306
32. S.H. Pereira, J.F. Jesus, Phys. Rev. D **79**, 043517 (2009). arXiv:0811.0099 [astro-ph]
33. D. Pavon, W. Zimdahl, Phys. Lett. B **628**, 206–210 (2005). arXiv:gr-qc/0505020
34. D. Pavon, B. Wang, Gen. Relativ. Gravit. **41**, 1–5 (2009). arXiv:0712.0565 [gr-qc]
35. W. Chen, Y.S. Wu, Phys. Rev. D **41**, 695–698 (1990). [erratum: Phys. Rev. D 45 (1992), 4728]
36. M.V. John, K.B. Joseph, Phys. Rev. D **61**, 087304 (2000). arXiv:gr-qc/9912069
37. S.G. Rajeev, Phys. Lett. B **125**, 144–146 (1983)
38. D. Brout, D. Scolnic, B. Popovic, A.G. Riess, J. Zuntz, R. Kessler, A. Carr, T.M. Davis, S. Hinton, D. Jones et al., Astrophys. J. **938**(2), 110 (2022). arXiv:2202.04077 [astro-ph.CO]
39. M. Moresco, L. Amati, L. Amendola, S. Birrer, J.P. Blakeslee, M. Cantiello, A. Cimatti, J. Darling, M. Della Valle, M. Fishbach et al., Living Rev. Relativ. **25**(1), 6 (2022). arXiv:2201.07241 [astro-ph.CO]
40. L. Chen, Q.G. Huang, K. Wang, JCAP **02**, 028 (2019). arXiv:1808.05724 [astro-ph.CO]
41. R.C. Nunes, S.K. Yadav, J.F. Jesus, A. Bernui, Mon. Not. Roy. Astron. Soc. **497**(2), 2133–2141 (2020). arXiv:2002.09293 [astro-ph.CO]
42. D. Foreman-Mackey, D.W. Hogg, D. Lang, J. Goodman, Publ. Astron. Soc. Pac. **125**, 306–312 (2013). arXiv:1202.3665 [astro-ph.IM]
43. A. Lewis, arXiv:1910.13970 [astro-ph.IM]
44. A. Bernui, E. Valentino, W. Giarè, S. Kumar, R.C. Nunes, Phys. Rev. D **107**(10), 103531 (2023). arXiv:2301.06097 [astro-ph.CO]
45. J.F. Jesus, R. Valentim, F. Andrade-Oliveira, JCAP **09**, 030 (2017). arXiv:1612.04077 [astro-ph.CO]

46. H. Akaike, IEEE Trans. Autom. Control **19**(6), 716–723 (1974)
47. G. Schwarz, Ann. Stat. **6**, 461–464 (1978)
48. Y. Yang, Y. Wang, X. Dai, Eur. Phys. J. C **85**(3), 224 (2025). arXiv:2502.17792 [astro-ph.CO]
49. D.M. Scolnic et al. [Pan-STARRS1], Astrophys. J. **859**(2), 101 (2018). arXiv:1710.00845 [astro-ph.CO]
50. A.G. Adame et al. [Desi], JCAP **02**, 021 (2025). https://doi.org/10.1088/1475-7516/2025/02/021. arXiv:2404.03002 [astro-ph.CO]
51. A. Gómez-Valent, J. Solà Peracaula, Phys. Lett. B **864**, 139391 (2025). arXiv:2412.15124 [astro-ph.CO]
52. A. Gomez-Valent, J. Solà Peracaula, Astrophys. J. **975**(1), 64 (2024). arXiv:2404.18845 [astro-ph.CO]